Applied Thermal Engineering 248 (2024) 123135

Contents lists available at ScienceDirect

Applied Thermal Engineering

journal homepage: www.elsevier.com/locate/apthermeng

Research Paper

Process control and energy saving in the ladle stage of a metal casting process through physics-based and ANN-based modelling approaches

Rita Mastrullo, Alfonso William Mauro *, Francesco Pelella, Luca Viscito

Department of Industrial Engineering, Università degli studi di Napoli – Federico II, P.le Tecchio 80, 80125 Naples, Italy

ARTICLE INFO

Keywords:
Ladle
Metal casting
Model predictive control
Heat losses
Artificial neural networks

ABSTRACT

The process and temperature control of metal casting applications is of utmost importance both to guarantee the good quality of the final product and also to pursue an energy saving policy. For this purpose, in this paper two different modelling approaches have been proposed to predict the liquid steel temperature inside a ladle for metal casting, shortly before the casting process. The first is a physics-based grey-box model relying on equations for the characterization of the heat transfer mechanisms inside the ladle structure, whereas the second approach relies on artificial neural networks (ANNs). Both methods have been calibrated with experimental data of a case study plant, and subsequently assessed and compared in terms of prediction accuracy. Results show that the physics-based approach is able to predict the casting temperature with a higher mean absolute error (MAE) of 14 °C, whereas the ANNs predictions result to be better, with MAEs around 6 °C. On the other hand, it has been demonstrated that the ANNs approach may lack of reliability, especially if input data strongly differ from the calibration dataset, whereas the physics-based approach results to be more consistent and trustworthy. Finally, an energy analysis is conducted to demonstrate the feasibility of the model in evaluating the potential energy saving compared with situations in which decisions are taken by operators without the aid of a model predictive control.

Nomenclature

Roman	
A	Surface area [m^2]
$\bar{b}_{I,II,o}$	Bias vector [-]
c	Heat capacity [J/kgK]
dx	Spatial integration step [m]
E	Energy [kWh]
$E_{min,process}$	Minimum energy needed to melt and heat the liquid steel [kWh]
E_n	Specific radiated power [W/m^2]
F_{12}, F_{13}, F_{23}	Radiative view factors [-]
h	Convective heat transfer coefficient [W/m^2K]

(*continued on next column*)

(*continued*)

Nomenclature

Roman	
A	Surface area [m^2]
Δh_{lv}	Latent heat [J/kg]
J	Radiosity [W/m^2]
J_o	Fictitious radiosity of the 0 point of the equivalent Y net [W/m^2]
k	Thermal conductivity [W/mK]
K_h	Proportional coefficient to the heat transfer coefficient h [$W/m^2K^{1.2}$]
m	Mass [kg]
N	Number of nodes/neurons [-]
$\dot{Q}$	Thermal Power [kW]

(*continued on next page*)

* Corresponding author.
E-mail address: wmauro@unina.it (A.W. Mauro).

https://doi.org/10.1016/j.applthermaleng.2024.123135
Received 19 December 2023; Received in revised form 26 March 2024; Accepted 6 April 2024
Available online 10 April 2024

(*continued*)

Nomenclature

Roman	
A	Surface area [m^2]
R_1, R_2, R_3, R_{12}, R_{13}, R_{23}	Thermal Radiative Resistances [m^{-2}]
R_a, R_b, R_c	Thermal Radiative resistance of the equivalent Y net [m^{-2}]
T	Temperature [°C]
Greek	
Δ	Variation [-]
ε	Emissivity [-]
θ	Generic time-step [s]
σ	Stephan-Boltzmann constant [W/m^2K^4]
Abbreviations	
ANN	Artificial Neural Network
BF	Blast Furnace
BOF	Basic Oxygen Furnace
CCM	Continuous casting machine
EAF	Electrical Arc Furnace
GA	Genetic Algorithm
ML	Machine Learning
VD	Vacuum Degassing
Subscripts	
amb	Ambient
back	Backfilling material
cb	Carbon bricks
conv	Convective
disp	Heat loss
ext	External
init	Initial
int	Internal
is	Insulation layer
lat	Lateral surface
liq	Liquid steel
melt	melting
mor	Cement mortar
op	Value chosen by the operator
rad	Radiative
safety	Safety lining
shell	External steel construction shell
top	Related to the top surface of the liquid steel
Statistic indexes	
Err_{max}	Maximum Error
Err_{min}	Minimum Error
Mean Absolute Error	$MAE = \frac{1}{N}\sum_{i=1}^{N}\lvert y_i - y_{pred,i}\rvert$
Mean Relative Error	$MRE = \frac{1}{N}\sum_{i=1}^{N}(y_i - y_{pred,i})$
$\delta_{\pm int}$	Percentage of points falling into the ± int error band
Std	Standard Deviation

1. Introduction

Metal casting is a manufacturing process where molten metal is poured into a mold and allowed to solidify, resulting in the formation of intricate metal components [1]. It has been employed for centuries and remains a primary method for producing parts with complex shapes that are difficult or expensive to create using other manufacturing techniques [2]. Among the future challenges facing this sector, efficient process control and temperature regulation are crucial. The main objectives, in fact, are to ensure high-quality final products, to minimize the wastes of material, and to achieve energy saving by reducing fuel and electricity consumptions in the melting and refining processes [3]. In terms of energy consumption, it has been estimated that only in the United States the energy utilized by metal casting facilities is 236 trillion Btu [4], whereas in the UK the energy burden for casting manufacturing process is around 38 to 67 MJ to produce 1 kg of casting [5], with about the 60–70 % required for the melting of the metal scraps [6,7]. A significant reduction in energy consumption needs to be achieved, particularly in the melting process, by reducing inefficiencies of furnaces, minimizing heat losses and non-processing time periods [8], and by reducing unnecessary superheating of molten metals [4] used to limit breakages in the casting process. Therefore, digital twins and predictive models would give a huge enhancement into the manufacturing and metal casting industry, by achieving better quality, higher productivity, lower costs and increased flexibility [9].

1.1. Description of a typical metal casting process

There are several intermediate steps needed to correctly melt the metal scraps and to realize the final product in a metal casting process. A preliminary phase consists of the storage and preparation of raw materials, such as various kinds of scrap metal (mostly alloy steel). The metal scrap is melted through a furnace which typically can be of three typologies: Blast Furnace (BF), Basic Oxygen Furnace (BOF) and Electrical Arc Furnace (EAF). BFs are typically used for iron production, whereas BOFs and EAFs are employed for the continuous casting and production of steel [10]. Worldwide, the EAF production method is preferred to the others due to the lower investment costs and a higher feasibility in the integration of steel production facilities, since the scrap steel is directly charged inside the EAF and an electrical arc is formed reaching temperatures over 1600 °C [11]. After approximately 90 min, the liquid steel is tapped into containers (ladles) and pass through a second phase of ladle furnace (LF). Besides transportation purposes, ladles are also needed to carry out secondary refining operations with the elimination of sulphurs, oxides and with the adjustment of the steel chemical composition and temperature before casting, improving the overall quality of the liquid steel [12] and reaching the target steel grade by adding especially calcium and aluminum [13]. The working principle of a LF is the same of an EAF, with the creation of big current electric arcs, generating the thermal energy to heat the steel [14]. A second refining could also occur through ad additional phase which is the vacuum degassing (VD), able to reduce the quantity of dissolved gas which can have a detrimental effect on the mechanical properties of the casting, by causing an overriding effect on the amount of porosity and distribution in the final product [15]. Once all the refining operations are completed, the steel is sent to the continuous casting machines (CCM), where the casting of the final product takes place. In this phase, the liquid steel from the ladle is tapped into a tundish, [16]. The nature of the final product depends on the typology of the shape, which can be of blooms and slabs [17]. An overview of all the phases of an entire metal casting process is provided in Fig. 1.

The transportation phases of the ladle before the casting process may depends on several constraints which are determined by the logistic of the production, and, typically, when a ladle remains stationary for a long time with a high temperature level, high heat losses are registered through the ladle walls and at the ladle top, especially when a cover is not employed [18]. Moreover, an accurate temperature control in the final casting operation is crucial to avoid segregation or, at worst, breakouts at excessively high temperatures, and steel contamination with macro-inclusion may occur at excessively low temperatures, causing at worst a solidification of the liquid steel inside the casting machine [19,20]. An accurate choice of the liquid steel temperature at

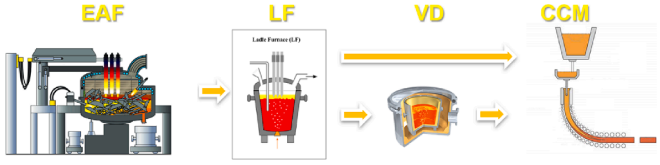

Fig. 1. Overview of an entire metal casting process with all the phases of Electric Arc Furnace (EAF), Ladle Furnace (LF), Vacuum Degassing (VD, Optional) and Continuous Casting Machine (CCM).

the end of the LF phase should therefore be considered, in order to have a right value between a certain tolerance at the beginning of the CCM process. Hence, a modelling of heat loss is of utmost importance to guarantee a high quality of the final product, without encounter risky conditions for the continuous operation of the machine and for the performance and productivity level of the entire process.

1.2. State of the art of predictive models, limits of the literature and objectives of the paper

There are several studies in the literature done in developing models to forecast the heat losses between the different phases of the metal casting processes and predicting the liquid steel temperature in the process. A list of literature works dealing with this topic is provided in Table 1, placed in chronological order from 2001 to 2024, by distinguishing on the columns the kind of employed modelling approach, an estimation of the computational time and the applicability for real-time monitoring, if the papers carry out a validation on experimental data or a comparison between different approaches. For further insights, the review works of Diniz et al. [16] and Chen et al. [21] can also be considered.

Some of the works presented, (Xia and Ahokainen [22], Ferreira et al. [23], Wu et al. [24], Siddiqui et al. [25]) develop multi-dimensional finite element models in order to investigate the thermal behaviour of the entire ladle (liquid steel and external structure), whereas others, such as the work of Pan et al. [18], compare different CFD (Computational Fluid Dynamics) approaches on the temperature field results. However, the employment of a 3D CFD or finite element model is usually suitable in a preliminary project and design phase and becomes not credible for predictive control due to the high computational time.

A real-time model would be instead more practical for control purposes, especially if results must be obtained in a short period of time. These kinds of models can be in divided into different categories, such as physics-based, grey-box, statistical, and machine learning based [26]. Very few works carry out a comparison between different modelling approaches, limiting the analysis only among models of the same kind by changing some parameters. For instance, Ahmad et al. [27] analyses different grey-box models among series, parallel and combined, whereas the works of Tian et al. [28] and He et al. [29] compares different ANN structures, analyzing their effect on the overall performance prediction. Only the work of Yuan et al. [30] proposes a comparison between physics-based approaches and artificial intelligence/machine learning methods in terms of prevision accuracy, whereas other papers analyze the possibility to employ ensemble hybrid physics-ML based models (Lü et al. [31,32], Ammar et al. [33]) in order to enhance the performance prediction compared to the individually applied approaches.

To the best of authors' knowledge, there are no other papers analyzing both of the two physics-based and ML-based real-time modelling approaches, not only comparing the two methods in terms of prediction accuracy, but also indicating lacks, limitations and possible application fields and zones for each of the investigated approaches.

Therefore, the main target of this paper is to deepen all the aforementioned features, and in detail to focus on the two following main aspects:

1) To carry out a comparison in term of prediction accuracy of two different modelling approaches able to predict the temperature evolution inside of a ladle for metal casting processes; the first relying on a physics-based approach which considers all the heat transfer mechanisms of conduction, convection and radiation, and the second based on the calibration of several artificial neural networks (ANNs).
2) To demonstrate the potentiality and applicability of each method in a practical use as model predictive control on a real plant facility with the aim to: a) optimize the management of the entire process; b) understand when it is better to use one or the other approach in dependence of the data availability; c) estimate the potential energy saving obtainable by employing a predictive model rather than standard control strategies based only on the operator experience. This point is also interesting for the implementation of a control strategy in which, depending on the external boundary conditions, the two approaches may operate in parallel to maximize the prediction accuracy in each zone of the external condition domain.

For both activities, field data of temperatures collected in different phases of the casting process have been used from a real case study of a foundry facility.

2. Field data availability and methods

2.1. Description of the database and schematic of the system modelled

The analyzed case study is a metal casting production industry (STOMANA Industry S.A.), and it is one of the case studies analyzed within the EnerMan H2020 European Project [49]. Temperature data of the liquid steel for each of the process phases described in Section 1.1 are collected. The system modelled is a traditional ladle for metal casting, being a cone-shaped structure made up of several layers. A layer of carbon ceramic bricks is employed to resist to very high temperatures and to limit thermal shocks in the tapping phases. For the case study analyzed, 4 different brick materials have been used for this layer, which will be referred as "Material 1 to 4", respectively from the top to the bottom of the ladle. To compensate the volume variations, a safety lining of Andalusite material is employed. A backfilling material is inserted between the carbon bricks and the safety lining to limit the encapsulation of air bubbles, which may expand causing creeks and breakages of the ladle, whereas an insulation layer is then applied to limit the heat losses. Finally, all layers are encapsulated in an external shell composed of stainless steel. The described stratigraphy is considered for both the lateral and the bottom surfaces, with the only difference that the backfilling material is not employed in the bottom parts of the ladle, and a layer of cement mortar between the insulation and the steel shell can instead be found. Moreover, due to the continuous tapping operations, no cover has been considered. A geometric representation of the ladle is provided in Fig. 2, with sections both on the longitudinal (Fig. 2(a)) and on the transversal directions, at different heights of the ladle (Fig. 2(b, c)). Other geometrical characteristics of the ladle are known; however, they cannot be provided due to company confidentiality issues.

All the thermodynamic properties in terms of density, heat capacity and thermal conductivity for all the materials employed in the different layers of the system analyzed are reported in Table 2. Particularly, some of these data are collected from several company datasheet, whereas some others are taken from literature.

2.2. Thermodynamic model equations

The model developed in this work considers several heat transfer equations for different zones of the ladle geometry, in order to evaluate all the heat losses and so the corresponding variation of the liquid steel temperature. Particularly, the model is 0D type for the liquid steel, whereas all the others heat transfer contributions through the ladle walls have been modelled with a 1D approach. All the heat losses are indicated in Fig. 3, in which each element has been numbered as follows. The external ambient and the liquid steel have been referred respectively as "amb" and "1". Number "2" refers to the portion of the ladle in which the brick layer is composed with material 1 and is not wetted by the liquid steel, whereas numbers "3" and "4" are related to the parts of the ladle composed of materials 1 and 2 respectively, both wetted by the liquid steel. Finally, numbers "5" and "6" are related to the bottom surfaces, both wetted by the liquid steel, in which the brick layer is composed of respectively materials 3 and 4. Regarding heat losses, two different convective contributions between the liquid steel volume and the

Table 1
State of the art of works dealing with predictive model in foundry aiming to estimate heat losses and temperatures in different phases of the metal casting process.

Article	Description	Kind of investigated model	Computational time	Results in real time	Validation on experimental data	Comparison among different modelling approaches
Xia and Ahokainen (2001) [22]	Model for the thermal stratification in the liquid steel considering turbulence and heat transfer	Physics-based	High	No	Yes	No
Ferreira et al. (2002) [23]	Finite element modelling of the ladle	Physics-based	High	No	Yes	No
Pan et al. (2003) [18]	1D, 2D CFD and 3D CFD models for the ladle heat losses	CFD	High	No	Yes	Yes
Gupta and Chandra (2004) [19]	Model to control the casting superheat temperature	Physics-based, statistical	Medium/Low	Yes	Yes	Yes
Camdali and Tunc (2006) [34]	Evaluation of heat losses from LF by conduction, convection, radiation	Physics-based	Medium	Yes	No	No
Dorcàk and Terpàk (2006) [35]	Online system for real time monitoring and prediction of liquid steel temperature in LF and CCM	Physics-based, statistical	Medium/Low	Yes	Yes	No
Tian et al. (2008) [28]	Temperature prediction in LF. Comparison between different ANN approaches	Hybrid physics-based /ANN	Medium/Low	Yes	Yes	Yes
Samuelsson and Sohlberg (2010) [20]	ODE model for the steel temperature estimation	Grey-box	Medium	Yes	Yes	No
Lü et al. (2012) [31 32]	Liquid steel temperature prediction in LF. Comparison between single ML and ensemble models	Hybrid physics-based/ML	Medium/Low	Yes	Yes	Yes
Sonoda et al. (2012) [36]	Statistical model to predict a probability distribution of liquid steel temperature in LF and CCM	Statistical	Low	Yes	Yes	No
Wu et al. (2012) [24]	Finite element model for the ladle process from preheating to turnover	Physics-based	High	No	Yes	No
Ahmad et al. (2014) [27]	Casting temperature prediction and control, with coefficient calibrated with statistical tool	Grey-box (parallel, serial, combined)	Medium	Yes	Yes	Yes
He et al. (2014) [29]	Prediction of the molten steel temperature in the process. Comparison between different ANN structure	Hybrid physic-based /ANN	Medium/Low	Yes	Yes	Yes
Laha et al. (2015) [37]	Models to predict the production efficiency depending on production and system parameters. Comparison of different ML methods	ML models	Low	Yes	Yes	Yes
Klanke et al. (2017) [38]	Methods to predict target meting temperature and carbon content of 10,000 plants. Comparison of different ML methods	ML models	Low	Yes	Yes	Yes
Wang et al. (2018) [39]	Integrated prediction and outlier detection of the temperature in the ladle from 17 inputs	Statistical	Low	Yes	Yes	No
Botnikov et al. (2019) [40 41]	Prediction of CCM initial temperature	ML, statistical	Low	Yes	Yes	No
Jo et al. (2019) [42]	Model to predict the endpoint temperature of molten steel. Comparison between ML models	Linear regression and ML models	Low	Yes	Yes	Yes
Song et al. (2019) [43]	Temperature prediction and control optimization in the ladle. Different ANN structure	ANNs	Low	Yes	Yes	No
Lee et al. (2020) [44]	Deep neural network based model to predict the temperature distribution in casting process	ANNs	Low	Yes	Yes	No
Siddiqui et al. (2021) [25]	Physics-based model for melt transfer, heat transfer, solidification in a steelmaking tundish	Physics-based	High	No	No	No
Yang et al. (2021) [45]	ML Model to preset the End-point Temperature of molten steel	ANNs	Low	Yes	Yes	No
Yuan et al. (2021) [30]	Ladle temperature prediction: comparison between physics-based and ML models	ANNs, CBR, hybrid ML/Physics-bases	Medium/Low	Yes	Yes	Yes
Neri and Lezzi (2023) [46]	Physics-based model for temperatures and energy demand for different working lining	Physics-based	Medium	Yes	No	No
Singh et al. (2023) [47]	ML models to predict process temperature in a BOF, LF and CCM	ML Models	Low	Yes	Yes	No
Sztangret et al. (2023) [48]	Prediction of Ladle Temperature: comparison of different ML methods	ANNs, ML models	Low	Yes	Yes	Yes
Ammar et al. (2024) [33]	Temperature prediction in casting: hybrid physics-based/ML approach to enhance prediction performance	Hybrid physic-based /ANN	Medium/Low	Yes	Yes	Yes

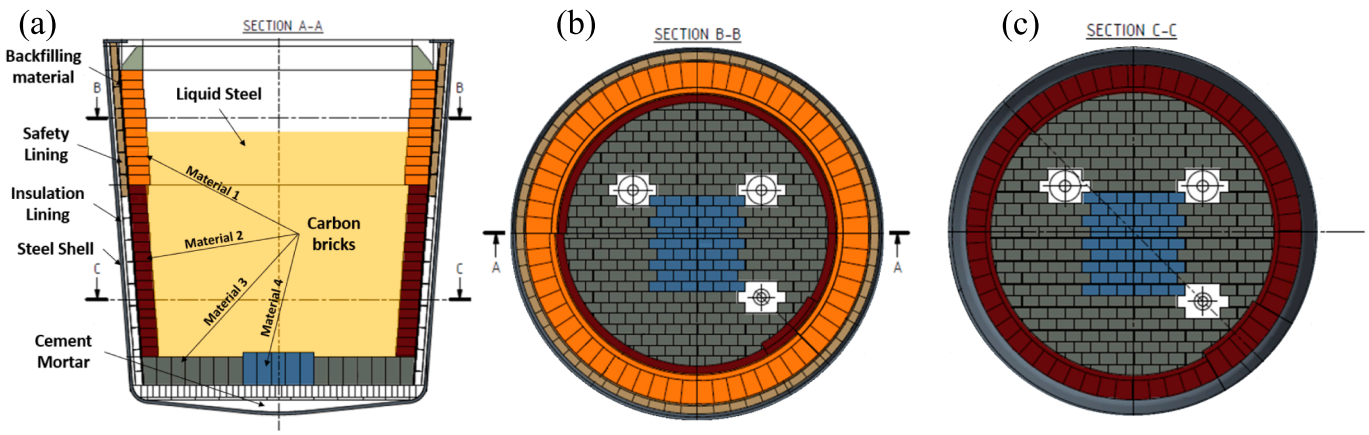

Fig. 2. Schematic of the ladle modelled in this work. (a) Longitudinal section. (b) Transversal section at the top of the ladle. (c) Transversal section at the bottom of the ladle.

Table 2
Main thermodynamic properties of materials composing the ladle structure considered in this work.

Property	Liquid Steel	Carbon Bricks				Backfilling	Safety Lining	Insulation	Cement mortar	Steel Shell
		Material 1	Material 2	Material 3	Material 4					
Density [kg/m^3]	7000	3030	3020	3070	3100	2000	2600	185	2200	7850
Heat Capacity [kJ/kgK]	0.365	1.3	1.3	1.3	1.3	0.88	1.3	1.65	0.90	0.49
Thermal conductivity [W/mK]	73	7.5	7.5	7	6.5	40	1.20	0.022	1.40	45
Source*	L [50,51]	SD	SD	SD	SD	SD/L [52]	SD/L [53]	SD/L [54]	L [55]	L [51,56]

*L: Literature; SD: Stomana Datasheet

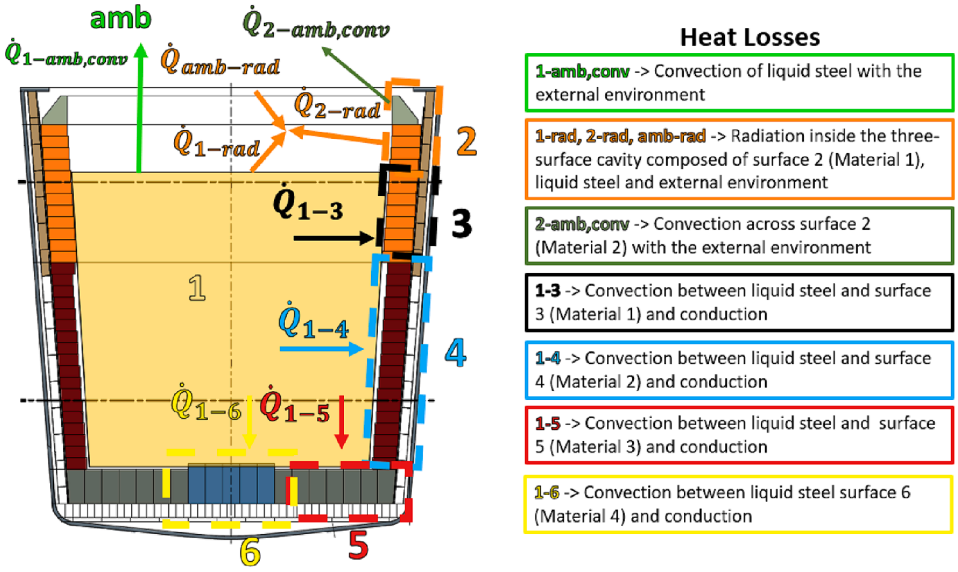

Fig. 3. Main heat losses contributions (conduction, convection, radiation) for each part of the layer structure considered for the thermodynamic modelling.

external environment ($\dot{Q}_{1-amb,conv}$) and between the surface "2" and the external environment ($\dot{Q}_{2-amb,conv}$) have been considered, whereas for the radiation, a mutual interaction of surfaces "1", "2", and "amb" has been taken into account by solving a three surface radiation problem, evaluating three different heat fluxes, named respectively as $\dot{Q}_{1-rad}$, $\dot{Q}_{2-rad}$, $\dot{Q}_{amb-rad}$. Finally, heat losses from the liquid steel across wetted surfaces, through respectively ladle parts "3", "4", "5", and "6" ($\dot{Q}_{1-3}$, $\dot{Q}_{1-4}$, $\dot{Q}_{1-5}$, $\dot{Q}_{1-6}$) are contemplated, by considering the convection on the internal surfaces with the liquid steel, and both convection and radiation with the external environment.

The distinction between zones "2" and "3" depends on the current level of the liquid steel free surface, estimated from the total mass of the liquid steel.

The overall variation of the liquid steel temperature has been calculated with an energy balance on the entire volume of the liquid steel, depending on the heat losses of the ladle, as shown in Eq.1:

$$m_{liq}c_{liq}\frac{dT_{liq}}{d\theta} = \left(\dot{Q}_{1-amb,conv} + \dot{Q}_{1-rad} + \dot{Q}_{1-3} + \dot{Q}_{1-4} + \dot{Q}_{1-5} + \dot{Q}_{1-6}\right) \quad (1)$$

With m_{liq} and c_{liq} being the total mass and specific heat of the liquid steel, whereas $d\theta$ is the current time-step. $\dot{Q}_{1-amb,conv}$, $\dot{Q}_{1-rad}$ and $\dot{Q}_{1-3}$ to $\dot{Q}_{1-6}$ are all the heat loss terms, evaluated as follows. For the convection between the liquid steel and the external ambient ($\dot{Q}_{1-amb,conv}$), Eq. (2) has been used:

$$\dot{Q}_{1-amb,conv} = h_{top}A_{top}(T_{liq} - T_{amb}) \quad (2)$$

h_{top} and A_{top} are respectively the heat transfer coefficient and the upper free surface of the liquid steel, whereas T_{liq} and T_{amb} are the liquid steel and ambient temperatures.

The mutual radiative interaction problem between the free surface of the liquid steel, the lateral surface 2 and the external ambient has been solved to evaluate $\dot{Q}_{1-rad}$, $\dot{Q}_{2-rad}$ and $\dot{Q}_{amb-rad}$, as shown in Fig. 4. Particularly, a truncated cone-shaped has been considered, with surface 1 and 2 related respectively to the liquid steel and the carbon brick, whereas surface 3 is representative of the external ambient. The equivalent radiation network with all the corresponding thermal resistances is provided in Fig. 4(b).

The heat fluxes $\dot{Q}_{1-rad}, \dot{Q}_{2-rad}$ and $\dot{Q}_{amb-rad}$ have been evaluated by solving the radiation net as a function of the temperatures of surfaces 1, 2 and the external ambient, and of the values assumed by the thermal resistances of the net, according to Eq. (3). The analytical solution of the equations system of the equivalent radiation net, as well as the equations for the evaluation of all the thermal resistances, are reported in Appendix.

$$\dot{Q}_{1-rad}, \dot{Q}_{2-rad}, \dot{Q}_{amb-rad} = f(T_1, T_2, T_{amb}, R_1, R_2, R_3, R_{12}, R_{13}, R_{23}) \quad (3)$$

The conduction inside the wall structure of the ladle has been solved to evaluate the remaining heat losses $\dot{Q}_{1-3}$ to $\dot{Q}_{1-6}$, as well as for the temperature of surface 2 needed to solve the mutual radiation problem presented above. A detail of the stratigraphy for each layer is presented in Fig. 5, in which Fig. 5(a) represents the layers for the lateral not-wetted surfaces ("2″), Fig. 5(b) for the lateral wetted surfaces ("3", "4"), whereas Fig. 5(c) for the bottom parts of the ladle ("5", "6"). For each layer, a 1D conduction problem has been solved, by discretizing the layers width for a certain number of nodes, indicated as $N_{cb}, N_{back}, N_{safety}$, N_{is}, N_{shell} and N_{mor} for respectively the carbon bricks, the backfilling, the safety, the insulation, the shell and the mortar layers, each spaced with a spatial step indicated with dx. All the edge effects have been neglected.

The equation system for each node and for a generic time θ are presented below (Eqs. (4)–(6)). All the equations have been employed considering an explicit resolution method.

$$\dot{Q}_{int} + \frac{kA}{dx}[T(2) - T(1)] = \frac{\mathrm{dm}c}{2d\theta}\left[T^{\theta+1}(1) - T^{\theta}(1)\right] \text{(Node 1, internal surface)} \quad (4)$$

$$\frac{kA}{dx}[T(i-1) - T(i)] + \frac{kA}{dx}[T(i+1) - T(i)] = \frac{\mathrm{dm}c}{d\theta}\left[T^{\theta+1}(i) - T^{\theta}(i)\right] \text{(Node i, internal)} \quad (5)$$

$$\frac{kA}{dx}[T(N-1) - T(N)] - \dot{Q}_{\mathrm{ext}} = \frac{\mathrm{dm}c}{2d\theta}\left[T^{\theta+1}(N) - T^{\theta}(N)\right] \text{(Node N, external surface)} \quad (6)$$

k is the thermal conductivity of the specific considered material, A is the surface area of the infinitesimal volume, which thickness is referred as dx. dmc is the heat capacity of the infinitesimal volume and, for the nodes at the border of each material, it has been evaluated considering half volume of the previous layer and the remaining half of the next. For generalization purposes, the internal heat losses $\dot{Q}_{1-3}$ to $\dot{Q}_{1-6}$ are indicated as $\dot{Q}_{int}$, whereas $\dot{Q}_{ext}$ refers to the convective and radiative heat fluxes between the external surface of the ladle shell and the external environment. $\dot{Q}_{int}$ and $\dot{Q}_{ext}$ are evaluated depending on the area of the considered surface, and on if it is wetted or not by the liquid steel, according to the equations reported in Table 3.

h_{ext}, h_{int} and ε_{lat} are respectively the external and internal conductive heat transfer coefficient, and surface emissivity, whereas σ is the Stephan-Boltzmann constant. T_{liq} is the actual temperature of the liquid steel, T_{amb} is the external ambient temperature, $T_{cb,i,int}$ is the temperature of the internal wall of the carbon bricks layer of the generic surface i, whereas $T_{sh,i,ext}$ is the temperature of the last node of the ladle shell. $A_{int,i}$ and $A_{ext,i}$ are respectively the internal and external heat transfer areas for the generic surface i.

Finally, for the evaluation of the heat transfer coefficients h_{ext}, h_{int} and h_{top}, Eqs. (7)–(9) have been employed, as a function of the average difference of temperature, in a similar form as suggested by correlations for the natural convection in the literature [57].

$$h_{int} = K_{h_{int}} \bullet \left(T_{liq} - T_{int}\right)^{0.2} \quad (7)$$

$$h_{ext} = K_{h_{ext}} \bullet \left(T_{ext} - T_{amb}\right)^{0.2} \quad (8)$$

$$h_{top} = K_{h_{top}} \bullet \left(T_{liq} - T_{amb}\right)^{0.2} \quad (9)$$

Overall, unknown constants of the model, such as $K_{hext}, K_{hint}, K_{htop}, \varepsilon_{lat}$, ε_{liq} have been calibrated on experimental data, as shown in Section 3.2

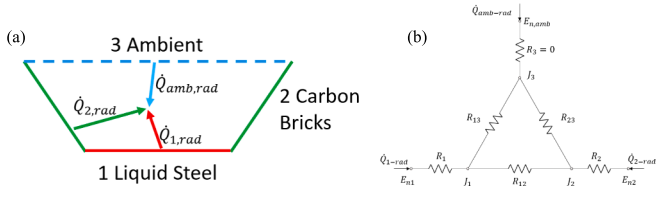

Fig. 4. (a) Schematic of the radiation problem between the liquid steel (red line), the carbon bricks (green line) and the external ambient (blue line, assuming a fictitious surface). (b) Equivalent radiation network of the problem.

2.3. Resolution algorithm

The resolution algorithm employed for the thermodynamic modelling approach is shown in Fig. 6. Particularly, after the ladle geometrical characterization, the liquid steel free surface level is evaluated, before dividing the ladle in parts "2″ to "6" defined in the section above. Then, the configuration factors and radiative thermal resistances for surfaces 1 and 2 are evaluated (Eqs. (13) to (15) in Appendix), and an initial condition for the dynamic simulation is chosen, as better clarified in Section 2.4. For each time step θ, the mutual radiation interaction network is firstly solved (Eqs. (3) and (16) to (21), reported in Appendix), then the conduction inside each layer is evaluated (Eqs. (4) to (6)) and finally the consecutive liquid steel temperature value is estimated through the energy balance on the entire liquid steel mass (Eq. (1)). The

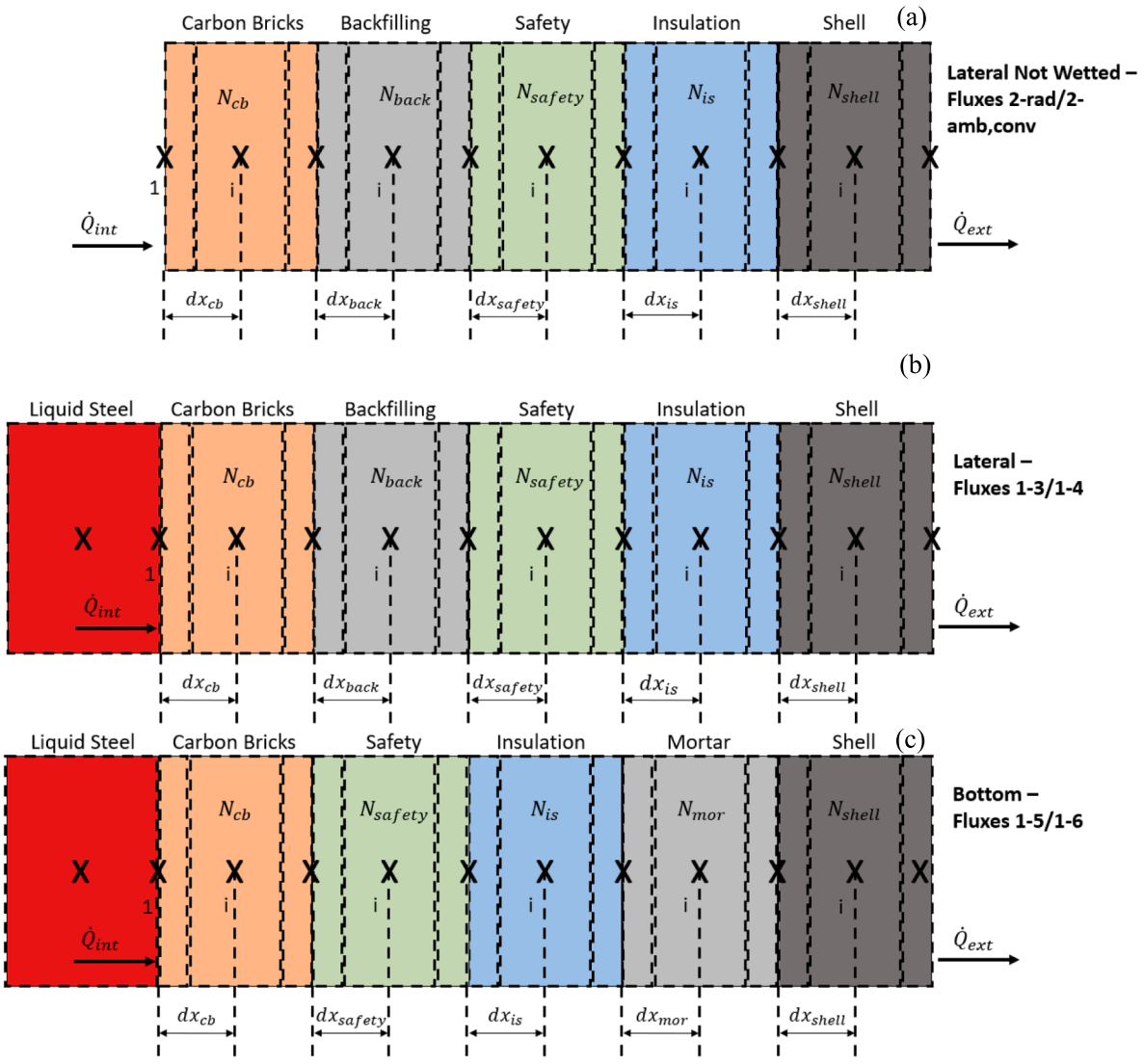

Fig. 5. Detail stratigraphy for each part of the ladle structure. (a) Lateral surfaces not wetted by the liquid steel. (b) Lateral surfaces wetted by the liquid steel. (c) Bottom surfaces wetted by the liquid steel.

Table 3
Equations for the evaluation of internal and external heat fluxes depending on the ladle surface number.

Surface number:	$\dot{Q}_{int}$	$\dot{Q}_{ext}$
2	$h^{*}_{ext}A_{int}\left(T_{amb}-T_{cb,2,int}\right)-\dot{Q}_{2-rad}$	$h_{ext}A_{ext,i}\left(T_{sh,i,ext}-T_{amb}\right)+$
3…6	$h_{int}A_{int,i}\left(T_{liq}-T_{cb,i,int}\right)$	$\varepsilon_{lat}A_{ext,i}\,\sigma\left[T^{4}_{\mathrm{sh,i,ext}}-T^{4}_{amb}\right]$

*Evaluated assuming the same heat transfer coefficient for the external convection (h_{ext})

same procedure is then applied for every consecutive time steps until the end of the simulation time, when the total decrease of the liquid steel temperature along a certain period of time can be estimated. The overall model has been implemented in MATLAB [58].

2.4. Dependencies on the initial condition and examples of temperature evolution

The results of the thermodynamic model strongly depend on the initial condition in terms of temperature of the entire ladle structure. However, this is always unknown from experimental data, therefore some actions should be applied to overcome this limitation. Particularly, two different approaches have been considered, referred in this work respectively as *case a* and *case b*.

- Case a: the initial condition for the entire ladle structure has been assumed equal to a steady-state conditions occurring by fixing the initial internal temperature of the liquid steel and solving the convection and conduction across the ladle structure.
- Case b: the initial condition for the entire ladle structure has been assumed equal to a steady-state condition occurring by fixing a uniform initial temperature of the internal walls for each material of the ladle structure. In this case, this temperature value becomes another parameter to be calibrated on experimental data.

Fig. 7 shows the initial temperature field for each material composing the entire ladle structure, depending on the total depth of the material itself, considering an example with an initial temperature of the liquid steel of 1613 °C, a total mass of liquid steel of 121 tons and an ambient temperature of 30 °C. Fig. 7(a) represents the temperature field for *case a*, whereas Fig. 7(b) for *case b*, by considering an internal wall temperature of 1000 °C. Other calibration constants of the thermodynamic model instead have been fixed arbitrarily and reasonably

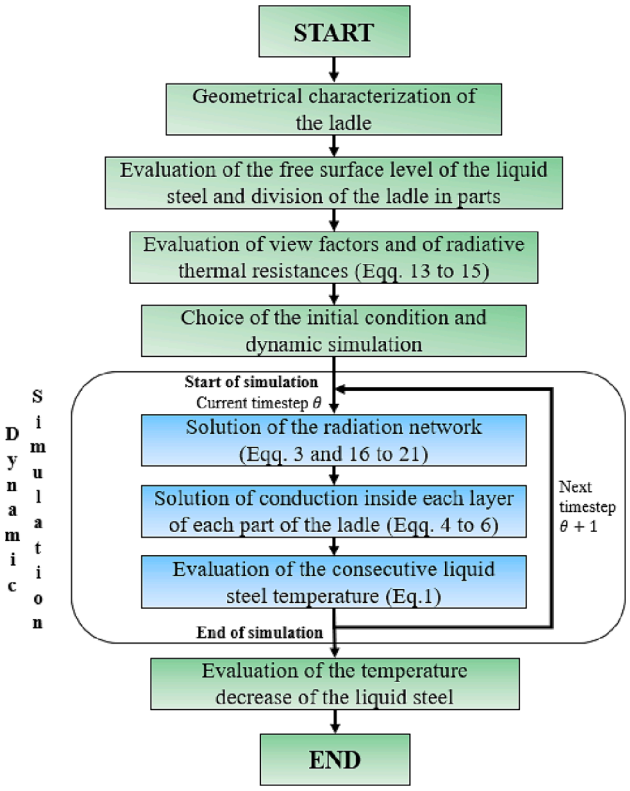

Fig. 6. Resolution Algorithm for the thermodynamic physics-based model.

($K_{h,ext} = 20$ W/m^{2}K$^{1.2}$; $K_{h,int} = 30$ W/m^{2}K$^{1.2}$; $K_{h,liq} = 20$ W/m^{2}K$^{1.2}$; $\varepsilon_{lat} = 0.4$; $\varepsilon_{liq} = 0.2$).

To show the real dependencies of the results from the initial condition, Fig. 8 shows the temperature decrease of the liquid steel due to heat losses along a time period of 5000 s, for both the *cases a* and *b*, considering as an example only one experimental point and executing the model with the same boundary conditions of the experimental point itself. In detail, *case a* is represented by the red line, whereas *case b* by the blue and green lines, for an internal wall temperature of 1200 °C and 1000 °C, respectively. It is worth noting that, considering the previously fixed calibration constants, an internal temperature slightly below 1000 °C would give the best prediction accuracy of the model for that point. However, it should be clarified that the one presented in Fig. 8 is only an illustrative example and does not want to demonstrate the accuracy of the model. As a matter of fact, an exhaustive calibration of all the constants is carried out in Section 3.2, and the accuracy of each case is shown in Figs. 11 and 12.

2.5. ANN models

Another approach based on ML has been developed for the system analyzed. Particularly, Artificial Neural Networks have been considered and a schematic example for the developed ANNs is provided in Fig. 9.

Each connection represents a weight, whereas each neuron is an activation function taking the sum of input signals from the previous layer and transferring it to the next one [59,60]. The red boxes represent the input layers, composed of N different inputs, whereas the blue circle is the output layer. Furthermore, the yellow rhombuses are related to the hidden layers, each of them characterized by a certain number of neurons (N_I, N_{II}), whereas the yellow circles below ($\bar{b}_I, \bar{b}_{II}, \bar{b}_o$) represent the bias vectors related respectively to the hidden and output layers.

In this work, 16 different ANNs able to predict the first CCM temperature have been assessed and compared in terms of prediction accuracy. They have been divided into 4 different groups which differ from the number of input variables, ranging from 3 to 7, and from the calibration database. The input choice for each group of ANN has been selected as a result of a preliminary sensitivity analysis between inputs and outputs, not reported in this paper for brevity. Other different characteristics of the ANNs are the number of hidden layers, among 2 or 3, and the number of neurons of each hidden layer, ranging between 4 and 25. The number of hidden layers and neurons have been chosen according to the Zhang Method [61], and to some other evidences of the literature [29,43]. Other features are provided in Table 4. Group (1) contains only one neural network characterized by three inputs (last temperature of the LF process, mass of the liquid steel and time interval between the end of LF and the start of CCM), calibrated with all the experimental points of the database. In group (2), three more inputs are added (time periods between the end of EAF and the start of LF, between the start and the end of LF, and between two consecutive starting time of a single ladle), with several ANNs calibrated only on 2019 data. Group (3) instead considers a new input indicating the number of usages before a maintenance renew operation of a ladle, with all the ANNs calibrated on the whole available dataset. Finally, ANNs belonging to group (4) have the same structure of group (2), with the only difference that they have been calibrated on data for which the number of usages for each ladle before maintenance is less than 50. The entire database has been divided in 70 % for training, 15 % for validation and 15 % for testing, as usually carried out also in other similar works and applications [62]. The ANNs have been developed by means of the MATLAB Deep Learning Toolbox, and the normalization of input data, needed when ANNs are used [63], is automatically applied by the software.

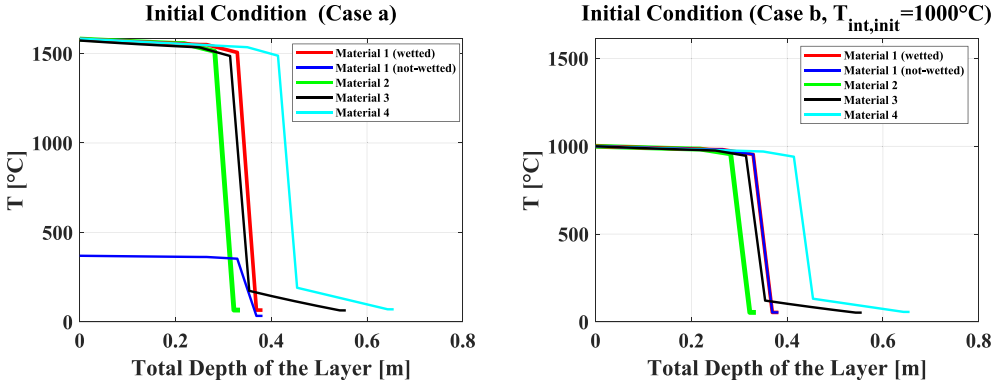

Fig. 7. Initial temperature profile inside each layer of the ladle structure, as a function of the total depth of the layer itself, for case a (a) and case (b) respectively, assuming an internal wall initial temperature of 1000 °C. For further details on materials 1 to 4 please refer to Fig. 2 and Table 2.

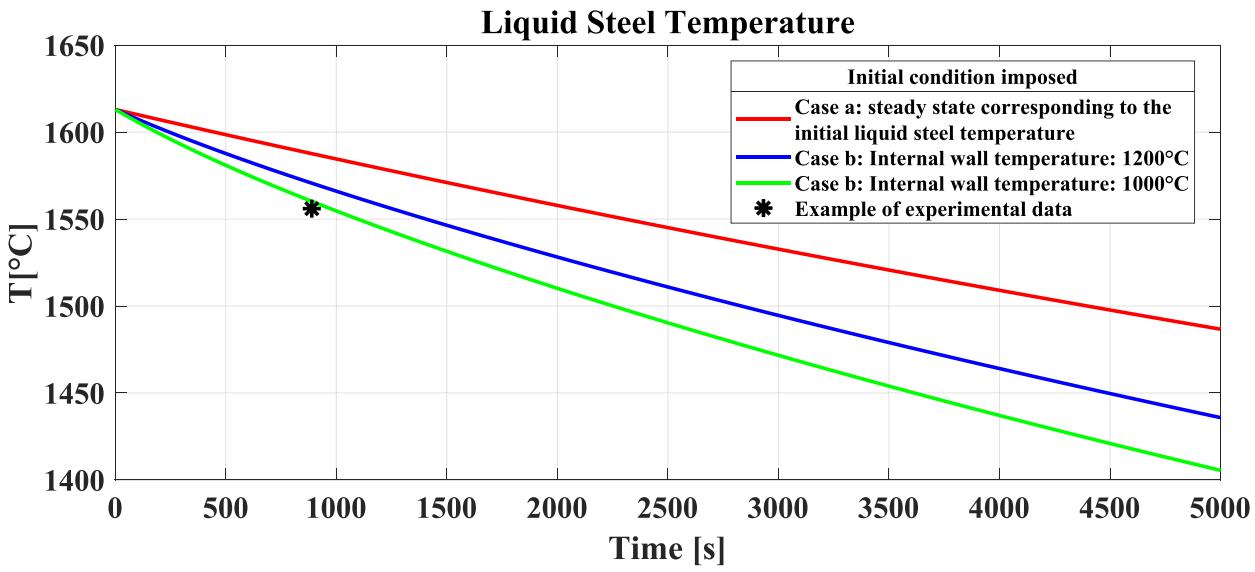

Fig. 8. Example of the dependence of the liquid steel temperature decrease by the initial condition, and comparison with an experimental point.

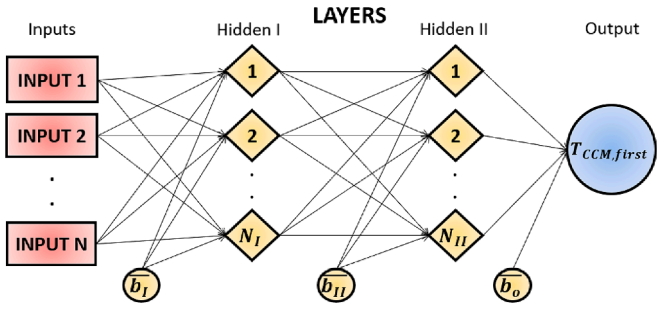

Fig. 9. Generic schematic of the ANNs structure considered in this work.

Table 4
List of ANNs considered in this paper, divided in 4 different groups depending on the number and type of Inputs and Outputs, the calibration database employed and the network structure.

Number	Inputs	Outputs	Net Structure*	Database
1	$T_{LF,last}$, m_{liq}, $\Delta\theta_{end,LF-start,CCM}$	$T_{CCM,first}$	3-20-20-1	All points (13200)
2.a	$T_{LF,last}$, m_{liq},		6-25-12-1	Point of the
2.b	$\Delta\theta_{end,LF-start,CCM}$, $\Delta\theta_{endEAF-startLF}$,		6-25-12-3-1	year 2019 (4400)
2.c	$\Delta\theta_{startLF-endLF}$,		6-12-12-1	
2.d	$\Delta\theta_{end,lastoperation,ladle}$		6-8-8-1	
2.e			6-4-4-1	
3.a	$T_{LF,last}$, m_{liq},		7-25-12-1	All points
3.b	$\Delta\theta_{endLF-startCCM}$, $\Delta\theta_{endEAF-startLF}$,		7-25-12-3-1	(13200)
3.c	$\Delta\theta_{startLF-endLF}$,		7-12-12-1	
3.d	$\Delta\theta_{end,lastoperation,ladle}$,		7-8-8-1	
3.e	Number of usages before renew		7-4-4-1	
4.a	$T_{LF,last}$, m_{liq},		6-25-12-1	All ladles with
4.b	$\Delta\theta_{endLF-startCCM}$, $\Delta\theta_{endTAP-startLF}$,		6-25-12-3-1	number of usages before
4.c	$\Delta\theta_{startLF-endLF}$,		6-12-12-1	renewing less
4.d	$\Delta\theta_{end,lastoperation,ladle}$		6-8-8-1	than 50 (1422)
4.e			6-4-4-1	

*in the form "x-a1-a2-..-an-y" in which "x" is the number of inputs, "y" the number of outputs, "a1, a2, an" are the number of neurons of each hidden layer, with n the number of hidden layers.

Table 5
Variation ranges for all the inputs and outputs of the investigated approaches, indicated in Table 4.

Variable	Minimum	Maximum	Average	Std
$T_{LF,last}$ [°C]	1527	1715	1598	25
m_{liq} [tons]	90	132	118	8
$\Delta\theta_{end,LF-start,CCM}$ [s]	600	5500	2092	1061
$\Delta\theta_{endEAF-startLF}$ [s]	100	4000	1204	903
$\Delta\theta_{startLF-endLF}$ [s]	150	10,500	4916	2663
$\Delta\theta_{end,lastoperation,ladle}$	1000	30,000	5929	5447
Number of usages before renew [-]	2	1162	328	265
$T_{CCM,first}$ [°C]	1490	1570	1541	11

3. Results

3.1. Experimental ranges of inputs and outputs

Table 5 shows a statistical overview of the variation ranges for each of the measured parameters of temperatures and time period between phases, reporting minimum, maximum, average values and standard deviation. It is worth noting that $T_{LF,last}$, $T_{CCM,first}$ and m_{liq} assume often similar values, whereas the ranges of the time periods between the different phases are broader. On the other hand, Fig. 10 shows an example of temperature evolution along all the metal casting processes, both in case of absence (Fig. 10(a)) and presence (Fig. 10 (b)) of the VD phase.

3.2. Calibration of the physics-based model and validation

For the physics-based model application, several unknown parameters for the evaluation of the internal and external convective heat transfer coefficients and for the emissivity of lateral and liquid steel surfaces have been calibrated on experimental data. Two different calibrations have been performed considering both *cases a* and *b* defined in Section 2.4, with the addition that in *case b* also the internal initial temperature has been considered as a variable to be calibrated. A genetic algorithm (GA) has been employed to find the optimal selection of calibration variables able to minimize the mean absolute error (MAE) between the experimental and predicted values for the first temperature of the CCM process. For the GA, the following hyperparameters have been considered: maximum generation of 200*number of input

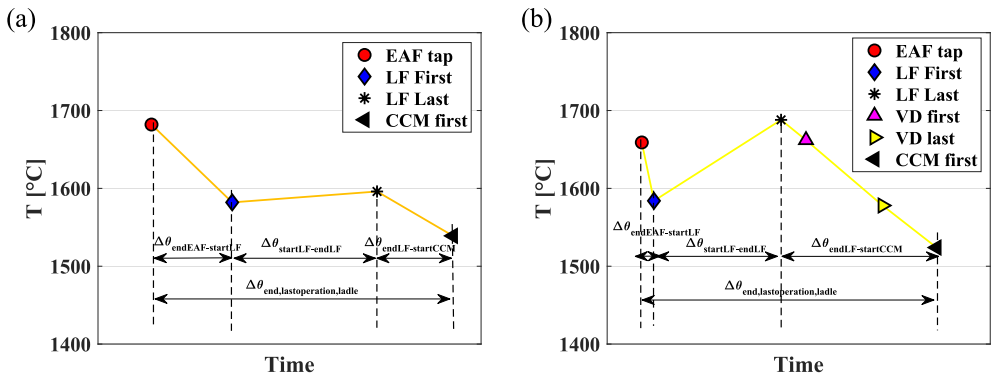

Fig. 10. Temperature evolution along all the metal casting processes for two different examples. (a) Absence of VD phase. (b) Presence of VD phase.

Table 6
Results for the calibration parameters of the thermodynamic model obtained through the GA for both the initial condition cases a and b.

Initial Condition Case	K_{hext} [W/m^{2}K$^{1.2}$]	K_{hint} [W/m^{2}K$^{1.2}$]	K_{htop} [W/m^{2}K$^{1.2}$]	ε_{lat} [-]	ε_{liq} [-]	$T^{\circ}_{int,init}$C
a	126.3	207.9	26.1	0.019	0.025	–
b	0.69	15.3	10.1	0.85	0.19	1276.3

variables, population size of 100, crossover fraction of 0.5, function tolerance of 10^{-4}. The following variation intervals for the calibration variables have been assumed:

- Proportional coefficient for the evaluation of the external convective heat transfer coefficient ($K_{h_{ext}}$) between 0.5 and 250 W/m^{2}K$^{1.2}$;
- Proportional coefficient for the evaluation of the internal convective heat transfer coefficient ($K_{h_{int}}$) between 10 and 500 W/m^{2}K$^{1.2}$;
- Proportional coefficient for the evaluation of the convective heat transfer coefficient at the free-surface of the liquid steel ($K_{h_{top}}$) between 0.5 and 250 W/m^{2}K$^{1.2}$;
- Emissivity of the lateral surface (ε_{lat}) between 0.01 and 1;
- Emissivity of the free surface of the liquid steel (ε_{liq}) between 0.01 and 1;
- Initial temperature of the internal surface of the ladle structure (only for *case b*) between 1000 and 1500 °C;

Results of the calibration parameters evaluated by the GA, for both *cases a* and *b* are presented in Table 6.

Result of the first CCM temperature experimental and predicted by the thermodynamic model is instead provided in Fig. 11. Statistic indexes in terms of mean absolute error (MAE), mean relative error (MRE), maximum (Err_{max}) and minimum (Err_{min}) errors, percentage of point falling within the error band $\pm 20^{\circ}C$ ($\delta_{\pm 20^{\circ}C}$) and standard deviation (Std) are also reported both in figures, and in Table 7. Particularly, for *case a* (Fig. 11(a)) the model is able to predict the temperature with a MAE of 13.3 °C, and a percentage $\delta_{\pm 20^{\circ}C}$ of 76.6 %. On the other hand, for *case b* (Fig. 11(b)) no improvements in terms of prediction accuracy are obtained, with a higher MAE of approximately 14 °C, and a slightly lower percentage $\delta_{\pm 20^{\circ}C}$ of about 76.2 %.

Therefore, the prediction of the model cannot ignore the initial conditions in terms of initial internal temperature of the ladle, since no potential improvements could be obtained by optimizing that variable. As a matter of fact, the prediction accuracy of the thermodynamic model could be significantly improved if the effective initial condition of the ladle, which is not currently measured in the analyzed case study, would have been known.

3.3. Validation of the ANN models

Results of the prediction accuracy for all the groups of ANNs defined in Table 4, in terms of predicted vs. experimental first CCM temperature are provided in Fig. 12. Fig. 12(a) shows the validation for the group (1), at which belongs only one neural network, whereas Fig. 12(b), (c) and (d) shows results for respectively groups (2), 3, and 4, each of them which includes 5 different ANNs.

Statistic indexes for each of the investigated ANNs are instead reported in Table 7. It is worth noting that, by increasing the number of inputs (passing from 3 of group (1) to (6) and 7 of respectively groups (2) and (3), a slight increase in prediction performance is registered (with MAE passing from 6.1 °C on average to 5.9 °C and $\delta_{\pm 20^{\circ}C}$ which remains almost constant with the value of 97.7 %), whereas a slight decrease of performance can be noted if only the ladles with a number of usage less than 50 are used (with a MAE of approximately 7.1 °C on average and $\delta_{\pm 20^{\circ}C}$ ranging between 96 % and 97 %. Regarding the choice of the ANNs structure, the numbers of neurons and hidden layers slightly affect the results, with a general tendency to marginally improve the prediction performance with more complex structures. Finally, the prediction performance obtained in predicting the experimental points by means of all the ANNs is higher than the ones for the thermodynamic model. In fact, the thermodynamic model results may be affected in a non-negligible way by other hidden effects such as unknown or not-measured data (e.g. initial conditions) and measuring equipment uncertainty. On the other hand, an ANN is able to directly incorporate all these effects by means of the calibration process on experimental data.

3.4. Lacks and limitations of the ANN-based approach

The developed models have been iteratively solved to estimate the optimal last LF temperature to be guaranteed. Particularly, the inputs in simulation mode are: the target first CCM temperature, the mass of liquid steel and the $\Delta time$ between the LF and CCM phases, whereas the output become the optimal last LF temperature. In order to analyze lacks and limitations of the analyzed approaches, the predictions of both models in terms of last LF temperature obtained for three experimental tests have been compared, as reported in Fig. 13. Particularly, the field data are represented with colored dots, whereas the dashed lines show the predictions of the model obtained considering as inputs the same

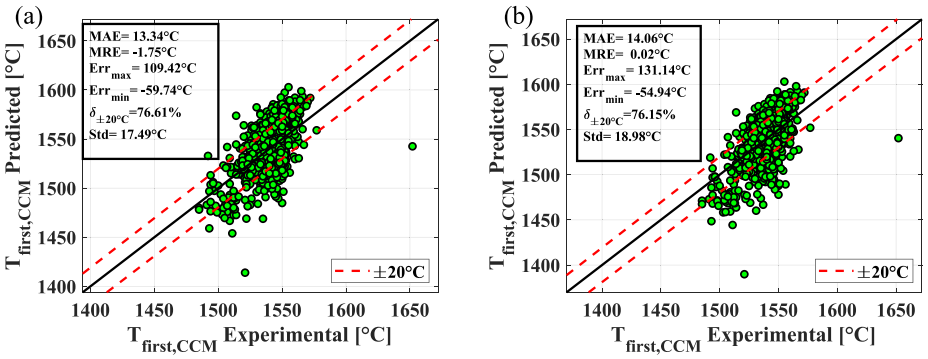

Fig. 11. Prediction accuracy of the physics-based approach in terms of first CCM temperature experimental vs. predicted, for both initial condition cases a (a) and b (b).

Table 7
Statistical indexes in terms of MAE, MRE, Err_{max}, Err_{min} $\delta_{\pm 20^{\circ}C}$, Std for the prediction accuracy of all the models analyzed in this work.

Model		*MAE*	[°C]*MRE* [°C]	Err_{max} [°C]	Err_{min} [°C]	$\delta_{\pm 20^{\circ}C}$[%]	*Std* [°C]
Physics-based	*Case a*	13.3	−1.75	109.4	−59.7	76.6	17.5
	Case b	14.1	0.02	131.1	−54.9	76.2	19.0
ANN-based	*1*	6.1	0.02	49.2	−116.0	97.7	8.2
	2.a	6.0	0.78	44.8	−57.9	97.6	8.0
	2.b	6.0	−0.02	49.4	−55.6	97.5	8.1
	2.c	5.9	−0.04	42.6	−58.0	97.8	7.9
	2.d	6.1	0.03	40.1	−56.9	97.2	8.2
	2.e	6.0	0.10	49.0	−58.9	97.6	8.1
	3.a	5.9	−0.09	48.4	−67.2	97.8	8.0
	3.b	5.8	−0.04	51.9	−61.4	97.8	7.9
	3.c	6.0	0.04	51.0	−60.7	97.7	8.0
	3.d	6.0	0.11	52.1	−63.3	97.7	8.0
	3.e	6.0	−0.04	54.5	−59.3	97.5	8.1
	4.a	6.9	−0.15	40.7	−45.8	96.7	9.1
	4.b	7.2	0.75	31.1	−45.7	96.8	9.2
	4.c	6.9	0.06	41.4	−35.4	97.1	8.9
	4.d	7.1	−0.26	36.5	−45.3	96.2	9.3
	4.e	7.2	−0.17	45.6	−44.2	96.3	9.5

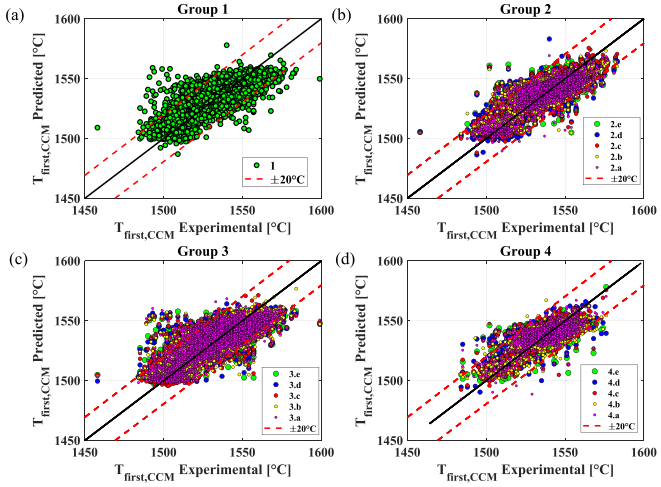

Fig. 12. Prediction accuracy of the ANN based approaches in terms of first CCM temperature experimental vs. predicted, for ANN groups (1) (a), 2 (b), 3 (c) and 4 (d) defined in Table 3

masses of liquid steel and first CCM temperatures of the experimental points, and values of time between the LF and CCM phases ranging from 0 to 1.5 h. It is worth noting that the Physics-based approach (Fig. 13(a)) is able to predict the experimental data with lower accuracy than the ANN-based approach (Fig. 13(b)), as evidenced also by results in Section 3.3. On the other hand, the ANN-based approach may give completely not-physical results, if queried for inputs which differ from the calibration dataset. For instance, according to the ANN, the last LF temperature does not change anymore for a $\Delta time_{LF-CCM}$ lower than 0.5 h, assuming constant values around 1600 °C, whereas it starts to decrease for a $\Delta time_{LF-CCM}$ higher than approximately 1.2 h.

Therefore, although a ML based approach could result in higher accuracy compared with traditional physics-based methods, the usage of ANNs could lead to completely unphysical and mistaken results, if they are used for inputs which are too far and different from the data used for the calibration.

3.5. Potential energy saving

Due to the limitations of the ANN approach, and a higher consistency and reliability of the physics-based model, this approach has been employed to perform an energy analysis, in order to evaluate the achievable energy saving, compared with a baseline scenario in which a non-optimal last LF temperature is chosen by an operator according to his experience without the aid of a predictive model. As a matter of fact, in this case the operator chooses a last LF temperature which is approximately 50 °C and 120 °C higher than the target temperature, respectively in case of absence and presence of the VD phase, in a way to avoid solidification effects before and during the casting process with high safety margins. The potential energy saved (ΔE_{saved}) has been evaluated as follows:

$$\Delta E_{saved} = m_{liq} \bullet c_{liq} \bullet \left(T_{lastLF,op} - T_{lastLF,optimal}\right) \quad (10)$$

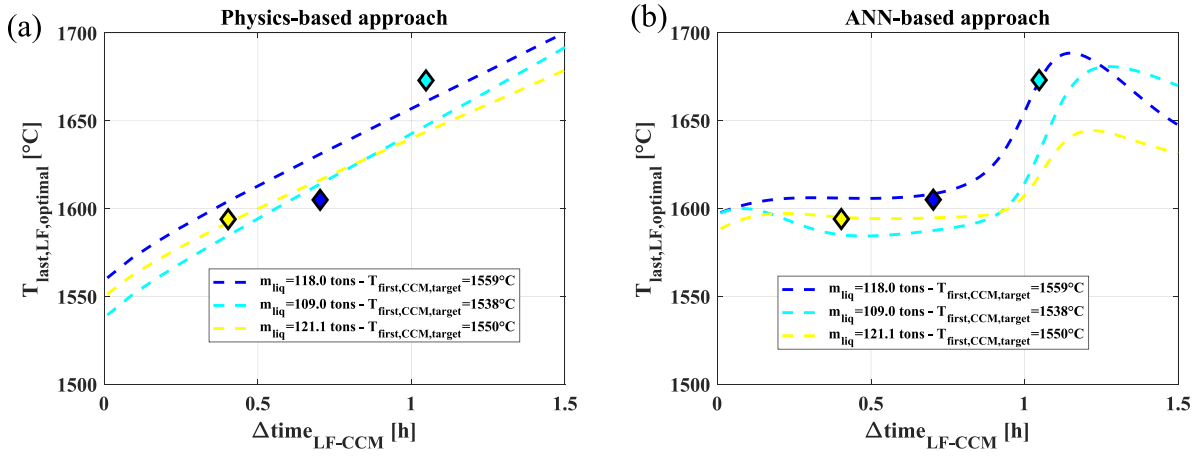

Fig. 13. Last LF temperature experimental (colored dots) and predicted by the physics-based (a) and ANN-based (b) approaches (dashed lines), for the same m_{liq} and $T_{first,CCM}$ of the experimental tests, as a function of the time between the LF and CCM phases.

Table 8
List of Inputs and Outputs employed for the energy analysis in the example provided in this section.

INPUTS		OUTPUTS	
m_{liq} [t]	100	$T_{last,LF,optimal}$ [°C]	1620.6
$T_{first,CCM,target}$ [°C]	1550	$T_{first,CCM,op}$ [°C]	1654.4
$T_{last,LF,op}$ [°C]	1750	ΔE_{saved} [kWh]	1311.9
$\Delta\theta_{end,LF-start,CCM}$ [s]	2000	E_{disp} [kWh]	715.9
T_{amb} [°C]	30	$E_{min,process}$ [kWh]	29,221
		$\Delta E_{saved}/E_{min,process}$ [%]	4.49
		$\Delta E_{disp}/E_{min,process}$ [%]	2.45

With m_{liq} the mass of the liquid steel, whereas $T_{lastLF,op}$ and $T_{lastLF,optimal}$ are the last LF temperature respectively chosen by the operator experience and the optimal evaluated through the model. On the other hand, the heat losses (E_{disp}), considering the optimal temperature profile of the liquid steel, have been estimated with the following relation:

$$E_{disp} = m_{liq} \bullet c_{liq} \bullet \left(T_{lastLF,optimal} - T_{firstCCM,target}\right) \tag{11}$$

Where $T_{firstCCM,target}$ is the target last CCM temperature to be reached. All these energy fluxes have been compared with a baseline energy consumption of the entire furnace process, considered as the minimum amount of energy needed to melt the liquid steel and heating it from the ambient temperature to the last LF optimal temperature, evaluated as follows:

$$E_{min,process} = m_{liq} \bullet \left[c_{solid}\left(T_{melt} - T_{amb}\right) + \Delta h_{lv} + c_{liq}\left(T_{lastLF,optimal} - T_{melt}\right)\right] \tag{12}$$

Where T_{melt} and Δh_{lv} are respectively the melting temperature and the fusion latent heat of the liquid steel. This contribution is the minimum amount of energy to provide to the entire furnace process and does not consider any other heat loss and inefficiencies of the EAF and LF respectively.

Results of the energy analysis are presented numerically in Table 8. Particularly, a mass of 100 t of liquid steel has been considered, with a target first CCM temperature of 1550 °C, and an idle time between the LF and CCM processes of 2000 s. Moreover, a non-optimal last LF temperature chosen by an operator of 1750 °C has been selected, and an ambient temperature of 30 °C. The model gives as outputs the optimal last LF temperature ($T_{last,LF,optimal}$) which is about 1621 °C, approximately 130 °C lower than the one chosen by the operator without the aid of the predictive model. Moreover, the first CCM temperature reached if the last LF temperature chosen by the operator ($T_{first,CCM,op}$) is approximately 105 °C higher than the target first CCM temperature value. Finally, all the energy fluxes are evaluated, as well as the ratios of the energy saved and dispersed on the minimum baseline energy.

Graphically, Fig. 14(a) shows a comparison of the liquid steel

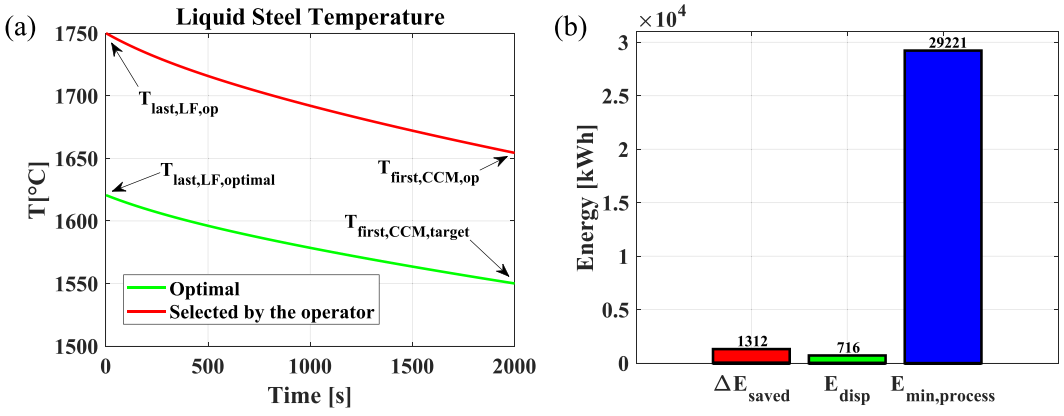

Fig. 14. (a) Liquid steel temperature decrease due to heat losses, considering the optimal last LF temperature (green profile) and a non-optimal choice made by an operator (red profile). (b) Energy fluxes in terms of energy saved (ΔE_{saved}), dispersed (E_{disp}) and baseline ($E_{min,process}$).

temperature decrease between the optimal profile (in green), obtained considering as first CCM temperature the optimal target value, and the one selected by the operator (in red), considering the last LF temperature chosen without the aid of the predictive model. Fig. 14(b) instead shows the results in terms of energy saved (in red), dispersed (in green) and minimum baseline to heat the liquid steel from the ambient to the optimal last LF temperatures (in blue). Overall, in this example the energy dispersed is 716 kWh, approximately 2.5 % of the baseline energy amount, whereas the energy saved results to be 1312 kWh, about the 4.5 % of the baseline.

A simple economic analysis has been carried out in order to estimate the potential cost savings deriving from the implementation and usage of the predictive model. In detail, it has been assumed that 10 equal casting processes occur during a single day (typical number for a metal casting company), and an electricity cost of 0.22 €/kWh has been considered (European average electricity cost for non-household consumers according to Eurostat [64]). Overall, a cost saving of about 2.89 k€ per day is obtained, against a total minimum amount of energy cost of 64.29 k€ per day to melt the entire mass of metal scraps.

4. Conclusions

Having at disposal a model in metal casting application able to predict the future behaviour of energy intensive systems would improve the control logics by enhancing energy saving opportunities in the field. In this paper two different approaches, physics-based and ANN based, have been proposed to model heat losses of a ladle used in foundry and to assess the temperature of the liquid steel shortly before the casting process. The key findings are outlined below:

- The physics-based grey-box model was developed based on fundamental heat transfer principles involving conduction, convection and radiation through the ladle structure. Two different scenarios, labeled as *case a* and *b*, were considered depending on the initial conditions set. The second approach instead comprises several ANNs, each differing in the number of inputs and outputs, as well as in the structure and in the calibration database.
- Both approaches were calibrated using experimental data from a real case study facility. Specifically, for the physics-based approach, various unknown constants were adjusted to minimize the mean absolute error (MAE) in predicting field data, while the ANNs were calibrated by partitioning the entire database in 70 % for training, 15 % for validation and 15 % for testing.
- Results show that, for *case a*, the thermodynamic approach can predict the experimental initial liquid steel casting temperature with a MAE of approximately 13 °C, with the 77 % of points falling within the error band $\pm 20^{\circ}C$. Conversely, no significant improvements were observed for *case b,* where MAE of the prediction is about 14 °C, with a $\delta_{\pm 20^{\circ}C}$ of approximately 76 %.
- In contrast, the ANN-based approach yields better prediction accuracy of the first CCM temperature, with a, average MAE of about 6 °C. Overall, while a slight improvement may be noticed by increasing the number of inputs for the prediction, the network structure (number of hidden layers and neurons) has a minimal influence on the overall prediction accuracy.
- Finally, the physics-based model was used to evaluate the potential energy saving compared to a baseline scenario where the decisions are made by an operator without a model predictive control. Particularly, it was found that, for 100 tons of liquid steel, if the operator considers a last LF temperature approximately 130 °C higher than the optimal value, an energy saving of approximately 1300 kWh can be achieved, equivalent to about the 4.5 % of the minimum baseline energy required to heat the same mass of liquid steel up to the optimal last LF temperature.

In conclusion, for this specific case study, the ANNs yields better performance in predicting the first CCM temperature rather than the physics-based approach. This may be attributed to the fact that thermodynamic model results are heavily influenced by the initial conditions of the ladle structure, which are not known from the experimental data of this case study. On the other hand, ANNs are capable of intrinsically incorporating all the missing information, leading to more accurate results. However, the use of ANNs may entail some risk, especially in extrapolating unphysical predictions beyond the calibration ranges, while the reliability of physics-based approaches, which never yield completely erroneous results, is usually higher in these conditions. Hence, employing both approaches in parallel would enhance the performance prediction and provide suggestions to the operators, that would be more conscious in making the right decisions. In this regard, the ANNs approach would operate effectively only in proximity of previously experimented boundary conditions, while for conditions significantly divergent from the norm, a physics-based approach could be employed for greater consistency. Furthermore, a physics-based approach could be used to conduct future scenario analyses, for instance change of production volume, change of temperature level etc., utilizing inputs data which completely differs from historical values. Finally, it should be noted that similar methods could be applied also to the remaining phases of the process. In future works we will consider the possibility to provide a complete “digital twin” able to optimize the entire process, further enhancing the system performance and the energy savings.

CRediT authorship contribution statement

Rita Mastrullo: Supervision. **Alfonso William Mauro:** Supervision, Resources, Methodology. **Francesco Pelella:** Writing – original draft, Investigation, Data curation. **Luca Viscito:** Writing – review & editing, Supervision, Methodology.

Declaration of competing interest

The authors declare that they have no known competing financial interests or personal relationships that could have appeared to influence the work reported in this paper.

Data availability

The data that has been used is confidential.

Acknowledgements

This research work was carried out as part of the ENERMAN (ENERgy-efficient manufacturing system MANagement) project founded by the European Union’s Horizon 2020 Program under Grant Agreement No. 958478.

Appendix

Solution of the mutual radiation problem between the liquid steel, the external ambient and the ladle structure

To solve the equivalent radiation net proposed in Fig. 4(b), the following transformation $\Delta \rightarrow Y$ has been applied, as shown in Fig. 15.

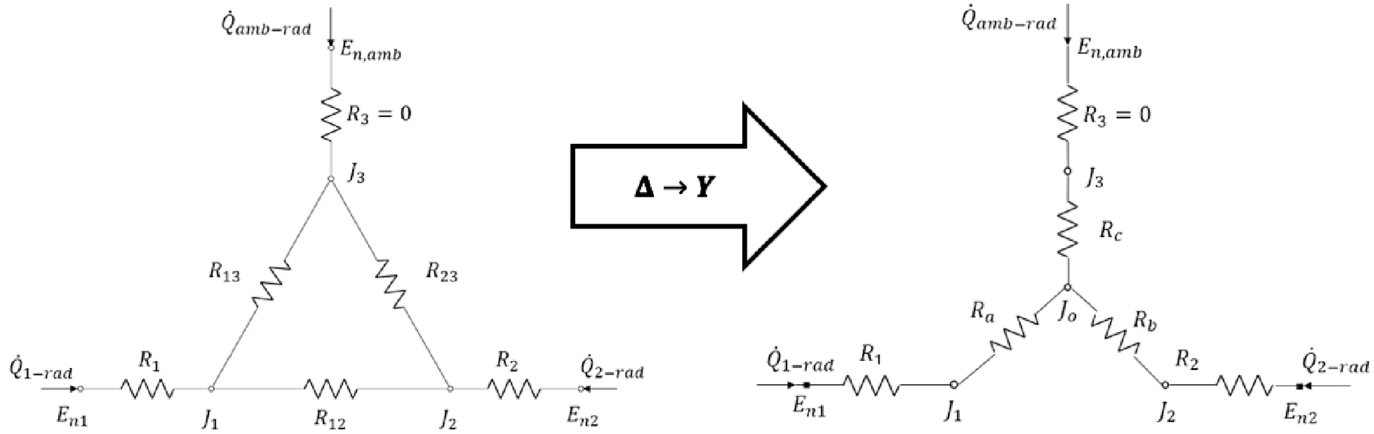

Fig. 15. transformation to the equivalent radiation network, able to simplify the resolution equation system

All the thermal resistances have been evaluated according to Baehr and Stephan [65] as shown in Eqs. (13) and (14):

$$R_1 = \frac{1-\varepsilon_{\text{liq}}}{A_{top} \bullet \varepsilon_{liq}}; R_2 = \frac{1-\varepsilon_{lat}}{A_{\text{int, 2}} \bullet \varepsilon_{lat}}; \; R_3 = \frac{1-\varepsilon_{\text{amb}}}{A_{\text{amb}} \bullet \varepsilon_{\text{amb}}} = 0; \tag{13}$$

$$R_{12} = \frac{1}{A_{top} \bullet F_{12}}; \quad R_{13} = \frac{1}{A_{top} \bullet F_{13}}; \quad R_{23} = \frac{1}{A_{\text{int,2}} \bullet F_{23}} \tag{14}$$

Particularly, due to the much higher surface of the external ambient compared with the others, the thermal resistance R_3 has been imposed equal to zero. Moreover, the configuration factors F_{12}, F_{13}, F_{23} have been evaluated according to [65], considering a truncate cone shape geometry.

The new resistances of the equivalent Y network can be evaluated according to Qin and Cheng (2003) [66], as shown in Eq. (15).

$$R_a = \frac{R_{13} \bullet R_{12}}{R_{13} + R_{23} + R_{12}} \qquad R_b = \frac{R_{23} \bullet R_{12}}{R_{13} + R_{23} + R_{12}} \qquad R_c = \frac{R_{13} \bullet R_{23}}{R_{13} + R_{23} + R_{12}} \tag{15}$$

Therefore, for each resistance of the equivalent Y network, the following equations (Eq. (16)) can be written:

$$\begin{cases} \dot{Q}_{1-rad} = \dfrac{E_{n1} - J_0}{R_1 + R_a} \\ \dot{Q}_{2-rad} = \dfrac{E_{n2} - J_0}{R_2 + R_b} \\ \dot{Q}_{amb-rad} = \dfrac{E_{n3} - J_0}{R_c} \\ \dot{Q}_{1-rad} + \dot{Q}_{2-rad} + \dot{Q}_{amb-rad} = 0 \end{cases} \tag{16}$$

J_0 is the fictitious radiosity the central point of the equivalent Y net, whereas E_{n1}, E_{n2} and E_{n3} are the specific radiated powers from each surface, which can be evaluated with the Stephan-Bolzmann Law [65], as shown in Eq. (17):

$$E_{n1} = \sigma \bullet T_1^4 \qquad E_{n2} = \sigma \bullet T_2^4 \qquad E_{n3} = \sigma \bullet T_3^4 \tag{17}$$

Considering as unknowns the three radiation heat fluxes from the three surfaces ($\dot{Q}_{1-rad}$, $\dot{Q}_{2-rad}$, $\dot{Q}_{amb-rad}$) and the fictitious radiosity J_0, the solutions of the linear systems are the ones of Eqs. (18)–(21):

$$\dot{Q}_{1-rad} = \frac{E_{n1}R_2 - E_{n3}R_2 + E_{n1}R_b - E_{n3}R_b + E_{n1}R_c - E_{n2}R_c}{R_1R_2 + R_2R_a + R_1R_b + R_1R_c + R_2R_c + R_aR_b + R_aR_c + R_bR_c} \tag{18}$$

$$\dot{Q}_{2-rad} = \frac{E_{n2}R_1 - E_{n3}R_1 + +E_{n2}R_a - E_{n3}R_a - E_{n1}R_c + E_{n2}R_c}{R_1R_2 + R_2R_a + R_1R_b + R_1R_c + R_2R_c + R_aR_b + R_aR_c + R_bR_c} \tag{19}$$

$$\dot{Q}_{amb-rad} = -\frac{E_{n1}R_2 + E_{n2}R_1 - E_{n3}R_1 - E_{n3}R_2 + E_{n2}R_a - E_{n3}R_a + E_{n1}R_b - E_{n3}R_b}{R_1R_2 + R_2R_a + R_1R_b + R_1R_c + R_2R_c + R_aR_b + R_aR_c + R_bR_c} \tag{20}$$

$$J_o = \frac{E_{n3}R_1R_2 + E_{n3}R_2R_a + E_{n3}R_1R_b + E_{n1}R_2R_c + E_{n2}R_1R_c + E_{n3}R_aR_b + E_{n2}R_aR_c + E_{n1}R_bR_c}{R_1R_2 + R_2R_a + R_1R_b + R_1R_c + R_2R_c + R_aR_b + R_aR_c + R_bR_c} \tag{21}$$

References

[1] P. Beeley, Foundry technology, Elsevier, 2021.
[2] S. Pattnaik, P.K. Jha, D.B. Karunakar, A review of rapid prototyping integrated investment casting processes, Proceedings of the Institution of Mechanical Engineers, Part l: Journal of Materials: Design and Applications 228 (4) (2014) 249–277.
[3] K. Salonitis, B. Zeng, H.A. Mehrabi, M. Jolly, The challenges for energy efficient casting processes, Procedia Cirp 40 (2016) 24–29.
[4] J. F. Schifo, J. T. Radia, Theoretical/best practice energy use in metalcasting operations (2004), Report available at http://www1. eere. energy. gov/industry/metalcasting/pdfs/doebestpractice_052804. pdf.
[5] B. Zeng, K. Salonitis, M.R. Jolly, Investigating the energy consumption of casting process by multiple life cycle method. International Conference on Sustainable Design and Manufacturing, 2014.
[6] M. Arasu, L.R. Jeffrey, Energy consumption studies in cast iron foundries. Transaction of 57th IFC, 2009.
[7] O.S.I. Fayomi, O. Agboola, S.O. Oyedepo, B. Ngene, N.E. Udoye, A Review of Energy Consumption in Foundry Industry, IOP Conf. Ser.: Earth Environ. Sci. 665 (2021) 012024. IOP Publishing.
[8] Z. Xu, Z. Zheng, X. Gao, Energy-efficient steelmaking-continuous casting scheduling problem with temperature constraints and its solution using a multi-objective hybrid genetic algorithm with local search, Appl. Soft Comput. 95 (2020) 106554.
[9] B. He, K.J. Bai, Digital twin-based sustainable intelligent manufacturing: a review, Adv. Manuf. 9 (2021) 1–21.
[10] D.M. Proctor, K.A. Fehling, E.C. Shay, J.L. Wittenborn, J.J. Green, C. Avent, R. D. Bigham, M. Connolly, B. Lee, T.O. Shepker, M.A. Zak, Physical and chemical characteristics of blast furnace, basic oxygen furnace, and electric arc furnace steel industry slags, Environ. Sci. Tech. 34 (8) (2000) 1576–1582.
[11] İ. Ekmekçi, Y. Yetisken, Ü. Çamdali, Mass balance modeling for electric arc furnace and ladle furnace system in steelmaking facility in Turkey, J. Iron Steel Res. Int. 14 (5) (2007) 1–6.
[12] T.A. Maia, V.C. Onofri, Survey on the electric arc furnace and ladle furnace electric system, Ironmak. Steelmak. 49 (10) (2022) 976–994.
[13] J.M. Manso, M. Losañez, J.A. Polanco, J.J. Gonzalez, Ladle furnace slag in construction, J. Mater. Civ. Eng. 17 (5) (2005) 513–518.
[14] S. Yanguang, W. Daixian, T. Baisheng, Y. Tao, S. Yang, F. Shubiao, W. Yuanhou, An intelligent ladle furnace control system. In Proceedings of the 3rd World Congress on Intelligent Control and Automation 1(2000), 330-334.
[15] G. Popescu, I. Gheorghe, F. Dănilă, P. Moldovan, Vacuum degassing of aluminium alloys, in: Materials Science Forum 217, Trans Tech Publications Ltd., 1996, pp. 147–152.
[16] A.P. Diniz, P.M. Ciarelli, E.O. Salles, K.F. Coco, Heat Transfer in Steel Ladles: Models and Applications. In Congresso Brasileiro de Automática-CBA 2(1)(2020).
[17] A. Tunuz, M. Furat, A Sensorless Crude Steel Cutting Method for Continuous Casting Machine. CILICIA International Symposium On Engineering and Technology CISET, Mersin, Turkey(2018), 19-22.
[18] Y. Pan, C.E. Grip, B. Björkman, Numerical studies on the parameters influencing steel ladle heat loss rate, thermal stratification during holding and steel stream temperature during teeming, Scand. J. Metall. 32 (2) (2003) 71–85.
[19] N. Gupta, S. Chandra, Temperature prediction model for controlling casting superheat temperature, ISIJ Int. 44 (9) (2004) 1517–1526.
[20] P. Samuelsson, B. Sohlberg, ODE-based modelling and calibration of temperatures in steelmaking ladles, IEEE Trans. Control Syst. Technol. 18 (2) (2009) 474–479.
[21] C. Chen, N. Wang, M. Chen, X. Yan, A framework based on heterogeneous ensemble models for liquid steel temperature prediction in LF refining process, Appl. Soft Comput. 131 (2022) 109724.
[22] J.L. Xia, T. Ahokainen, Transient flow and heat transfer in a steelmaking ladle during the holding period, Metall. Mater. Trans. B 32 (2001) 733–741.
[23] N.F. Ferreira, B.R. Henriques, D.S. Severo, O Modelo Matemático Das Panelas Da Cst, Santos, 2002.
[24] P.F. Wu, A.J. Xu, N.Y. Tian, D.F. He, Steel temperature compensating model with multi-factor coupling based on ladle thermal state, J. Iron Steel Res. Int. 19 (5) (2012) 9–16.
[25] M.I.H. Siddiqui, A. Maurya, F. Asiri, R. Kumar, Mathematical modeling of continuous casting tundish: a review, VW Appl. Sci 3 (1) (2021) 92–103.
[26] F. Pelella, L. Viscito, F. Magnea, A. Zanella, S. Patalano, A. W. Mauro, N. Bianco, Comparison between Physics-Based Approaches and Neural Networks for the Energy Consumption Optimization of an Automotive Production Industrial Process, Energies, 16(19)(2023) 6916.
[27] I. Ahmad, M. Kano, S. Hasebe, H. Kitada, N. Murata, Gray-box modeling for prediction and control of molten steel temperature in tundish, J. Process Control 24 (4) (2014) 375–382.
[28] H. Tian, Z. Mao, Y. Wang, Hybrid modeling of molten steel temperature prediction in LF, ISIJ Int. 48 (1) (2008) 58–62.
[29] F. He, D.F. He, A.J. Xu, H.B. Wang, N.Y. Tian, Hybrid model of molten steel temperature prediction based on ladle heat status and artificial neural network, J. Iron Steel Res. Int. 21 (2) (2014) 181–190.
[30] F. Yuan, A.J. Xu, M.Q. Gu, Development of an improved CBR model for predicting steel temperature in ladle furnace refining, Int. J. Miner. Metall. Mater. 28 (2021) 1321–1331.
[31] W. Lü, Z.Z. Mao, P. Yuan, Ladle furnace liquid steel temperature prediction model based on optimally pruned bagging, J. Iron Steel Res. Int. 19 (12) (2012) 21–28.
[32] W. Lü, Z. Mao, P. Yuan, M. Jia, Multi-kernel learnt partial linear regularization network and its application to predict the liquid steel temperature in ladle furnace, Knowl.-Based Syst. 36 (2012) 280–287.
[33] A. Ammar, M. Ben Saada, E. Cueto, F. Chinesta, Casting hybrid twin: physics-based reduced order models enriched with data-driven models enabling the highest accuracy in real-time, Int. J. Mater. Form. 17 (2) (2024) 1–17.
[34] Ü. Çamdali, M. Tunc, Steady state heat transfer of ladle furnace during steel production process, J. Iron Steel Res. Int. 13 (3) (2006) 18–25.
[35] Ľ. Dorčák, J. Terpak, Monitoring and prediction of the liquid steel temperature in the ladle and tundish, Metalurgija 45 (2) (2006) 93–96.
[36] S. Sonoda, N. Murata, H. Hino, H. Kitada, M. Kano, A statistical model for predicting the liquid steel temperature in ladle and tundish by bootstrap filter, ISIJ Int. 52 (6) (2012) 1086–1091.
[37] D. Laha, Y. Ren, P.N. Suganthan, Modeling of steelmaking process with effective machine learning techniques, Expert Syst. Appl. 42 (10) (2015) 4687–4696.
[38] S. Klanke, M. Löpke, N. Uebber, H.J. Odenthal, J. Van Poucke, A. Van Yperen-De Deyne, Advanced data-driven prediction models for BOF endpoint detection, in: Association for Iron & Steel Technology 2017 Proceedings, 2017, pp. 1307–1313.
[39] B. Wang, Z. Mao, K. Huang, A prediction and outlier detection scheme of molten steel temperature in ladle furnace, Chem. Eng. Res. Des. 138 (2018) 229–247.
[40] S.A. Botnikov, O.S. Khlybov, A.N. Kostychev, Development of a steel temperature prediction model in a steel ladle and tundish in a casting and rolling complex, Steel Transl. 49 (10) (2019) 688–694.
[41] S.A. Botnikov, O.S. Khlybov, A.N. Kostychev, Development of the metal temperature prediction model for steel-pouring and tundish ladles used at the casting and rolling complex, Metallurgist 63 (7–8) (2019) 792–803.
[42] H. Jo, H.J. Hwang, D. Phan, Y. Lee, H. Jang, Endpoint Temperature Prediction Model for LD Converters Using Machine-Learning Techniques April (2019) 22–26.
[43] G.W. Song, B.A. Tama, J. Park, J.Y. Hwang, J. Bang, S.J. Park, S. Lee, Temperature control optimization in a steel-making continuous casting process using a multimodal deep learning approach. steel research international, 90(12)(2019) 19003.
[44] S.Y. Lee, B.A. Tama, C. Choi, J.Y. Hwang, J. Bang, S. Lee, Spatial and sequential deep learning approach for predicting temperature distribution in a steel-making continuous casting process, IEEE Access 8 (2020) 21953–21965.
[45] J. Yang, J. Zhang, W. Guo, S. Gao, Q. Liu, End-point temperature preset of molten steel in the final refining unit based on an integration of deep neural network and multi-process operation simulation, ISIJ Int. 61 (7) (2021) 2100–2110.
[46] M. Neri, A.M. Lezzi, Energy demand in secondary steel making process: numerical analysis to assess the influence of the ladle working lining properties. In Journal of Physics: Conference Series (2023)(Vol. 2509, No. 1, p. 012003). IOP Publishing.
[47] M.K. Singh, A. Choudhury, D. Uikey, S. Pal, Correlation and prediction of molten steel temperature in steel melting shop using reliable machine Learning (RML) approach, Trans. Indian Inst. Met. (2023) 1–13.
[48] Ł. Sztangret, K. Regulski, M. Pernach, Ł. Rauch, Prediction of Temperature of Liquid Steel in Ladle Using Machine Learning Techniques. Coatings, 13(9)(2023), 1504.
[49] Enerman, 'EnerMan H2020 - Energy Efficient Manufacturing System Management', EnerMan, 2022. https://enerman-h2020.eu/ (accessed Jul. 12, 2022).
[50] M. Rywotycki, Z. Malinowski, J. Giełżecki, A. Gołdasz, Modelling liquid steel motion caused by electromagnetic stirring in continuous casting steel process, Arch. Metall. Mater. 59 (2014).
[51] C. S. Kim, Thermophysical properties of stainless steels (No. ANL-75-55). Argonne National Lab. (1975), Ill.(USA).
[52] NIST Chemistry WebBook SRD69 (https://webbook.nist.gov/chemistry/). Accessed on data 04/10/2023.
[53] M.W. Chase, NIST-JANAF Themochemical Tables, Fourth Edition, J. Phys. Chem. Ref. Data, Monograph 9 (1998), 1-1951.

[54] Y. Yousefi, F. Tariku, Thermal conductivity and specific heat capacity of insulation materials at different mean temperatures. In Journal of Physics: Conference Series (2021, November), Vol. 2069, No. 1, p. 012090. IOP Publishing.
[55] A. Stolarska, J. Strzałkowski, The thermal parameters of mortars based on different cement type and W/C ratios. Materials 13(19)(2020), 4258.
[56] The Engineering ToolBox (2005). Metals, Metallic Elements and Alloys - Thermal Conductivities. [online] Available at: https://www.engineeringtoolbox.com/thermal-conductivity-metals-d_858.html [Accessed Day Month Year].
[57] H.D. Baher, K. Stephan, Convective heat and mass transfer. Single phase flow, Heat Mass Transf. (2011) 275–441.
[58] MATLAB release. Natick, Massachussets, United States, The MathWorks, Inc.
[59] S. C. Wang, Interdisciplinary computing in Java programming (Vol. 743). Chapter 5: Artificial Neural Network. Springer Science & Business Media (2003).
[60] E. Guresen, G. Kayakutlu, Definition of artificial neural networks with comparison to other networks, Procedia Comput. Sci. 3 (2011) 426–433.
[61] L.M. Zhang, Models and applications of artificial neural networks, Fudan University Press, Shanghai, 1992.
[62] The MathWorks, Inc, Divide Data for Optimal Neural Network Training, https://it.mathworks.com/help/deeplearning/ug/divide-data-for-optimal-neural-network-training.html. Accessed in data: 10/02/2024.
[63] V. Farzaneh, A. Ghodsvali, H. Bakhshabadi, Z. Dolatabadi, F. Farzaneh, I. S. Carvalho, K. Sarabandi, Screening of the alterations in qualitative characteristics of grape under the impacts of storage and harvest times using artificial neural network, Evol. Syst. 9 (2017) 81–89.
[64] Eurostat, Electricity prices (including taxes) for household consumers, second half 2021, https://ec.europa.eu/eurostat/statistics-explained/index.php?title=Electricity_price_statistics#:~:text=The%20EU%20average%20price%20in,was%20%E2%82%AC0.2369%20per%20kWh.
[65] H.D. Baehr, K. Stephan, Thermal radiation, Heat Mass Transf. (2011) 545–658.
[66] Z. Qin, C.K. Cheng, Linear network reduction via generalized Y-Δ transformation: applications. technical report (2003) University of California, San Diego.